University of Plymouth

PEARL **https://pearl.plymouth.ac.uk**

Faculty of Science and Engineering School of Engineering, Computing and Mathematics

2022-09-01

Towards a new methodology for the characterisation of crack tip fields based on a hybrid computational approach

Camacho-Reyes, A

http://hdl.handle.net/10026.1/19328

10.1016/j.ijfatigue.2022.106942
International Journal of Fatigue

All content in PEARL is protected by copyright law. Author manuscripts are made available in accordance with publisher policies. Please cite only the published version using the details provided on the item record or document. In the absence of an open licence (e.g. Creative Commons), permissions for further reuse of content should be sought from the publisher or author.

International Journal of Fatigue 162 (2022) 106942

Contents lists available at ScienceDirect

International Journal of Fatigue

journal homepage: www.elsevier.com/locate/ijfatigue

Towards a new methodology for the characterisation of crack tip fields based on a hybrid computational approach

A. Camacho-Reyes [a], J.M. Vasco-Olmo [a,*], M.N. James [b,c], F.A. Diaz [a]

[a] Departamento de Ingeniería Mecánica y Minera, Universidad de Jaén, Jaén, Spain
[b] School of Engineering, Computing and Mathematics University of Plymouth, Plymouth, England, United Kingdom
[c] Department of Mechanical Engineering, Nelson Mandela Metropolitan University, Port Elizabeth, South Africa

ARTICLE INFO

Keywords:
Crack tip fields
Crack tip characterising parameters
CJP model, hybrid optimisation
Crack tip location, genetic algorithm

ABSTRACT

This work presents a hybrid optimisation technique for the simultaneous calculation of crack tip characterising parameters and its spatial location, which can significantly affect the characterising parameters if the position used is inaccurate. The hybrid technique combines initial use of a genetic algorithm to obtain a well-conditioned set of initial parameter values that is then passed to an interior point optimisation algorithm for subsequent fast optimisation. Use of the hybrid technique is also amenable to easy automation. The capability of the technique is demonstrated using the CJP crack tip field model, with digital image correlation (DIC) being used to measure the 2D crack tip displacement field. This model was chosen, not only for its demonstrated sensitivity to accuracy in crack tip location, but also for its proven utility in providing effective crack growth correlation in the presence of plasticity-induced shielding across a wide range of growth rates. The results obtained from the hybrid technique are shown to be reliable through comparison with results obtained using other established techniques.

1. Introduction

The development of full field optical techniques, such as Digital Image Correlation (DIC) [1], Thermoelastic Stress Analysis (TSA) [2] or Digital Photoelasticity [3], in combination with analytical mathematical models describing crack tip fields, have made it possible to experimentally determine characterising parameters, including the stress intensity factor (SIF) and T-stress, and to better understand their role in the mechanisms driving fatigue crack growth. The Multi-Point Over Deterministic Method (MPODM) developed by Sanford and Dally [4] has underpinned a large body of work aimed at improving understanding of fatigue crack growth where these optical techniques have been combined with various crack tip field models, e.g. the Irwin-Westergaard approach [5,6], Williams' expansion series model [7], complex Fourier analysis [8] the Muskhelishvili approach [9], a displacement partitioning model [10], and the model developed by Christopher James and Patterson (known as CJP model) [11–13]. Depending on what crack tip field (stresses, strains or displacements) is under consideration, as well as which variables and parameters are considered in the fitting process, the mathematical problem can be either linear or nonlinear.

Analytical methods can be used to solve the problem if the mathematical formulation is linear, while numerical methods are necessary to solve cases where the mathematical formulation is nonlinear. Published literature includes a number of studies where displacement data is used in crack tip field research without considering the crack tip location as an initially unknown quantity. For instance, Lopez-Crespo et al [14] employed the mathematical formulation developed by Nurse and Patterson [8] which is based on Muskhelishvili's complex potentials [9], Yates et al [15] used Williams' expansion series [7] and Vasco-Olmo et al [16] compared the Irwin-Westergaard [5,6], Williams' [7], and CJP models [11–13]. All of these studies considered only the crack tip singularity parameters as unknowns in the analytical definition of the crack tip field and hence a system of linear equations was obtained that could be easily solved using direct methods. In addition, in those cases where displacement data and purely elastic models (Westergaard, Williams or Muskhelishvili) are employed, the methodology is robust in terms of the crack tip position chosen for the fitting process, since a crack tip value close to the real one can provide reliable results in terms of singularity characterising parameters.

However, the CJP model is very sensitive to crack tip location [17]. The fitting process of the model to experimental data is therefore more complex than is the case for the other models, since the approach models a novel 'plastic inclusion' that explicitly incorporates the interaction effects at the boundary between the plastic and elastic regions [13]. Including the crack tip location as an unknown in the mathematical

* Corresponding author.
E-mail address: jvasco@ujaen.es (J.M. Vasco-Olmo).

https://doi.org/10.1016/j.ijfatigue.2022.106942
Received 14 January 2022; Received in revised form 25 March 2022; Accepted 18 April 2022
Available online 22 April 2022
0142-1123/© 2022 The Authors. Published by Elsevier Ltd. This is an open access article under the CC BY-NC-ND license (http://creativecommons.org/licenses/by-nc-nd/4.0/).

Nomenclature

u, v	Displacement field
G	Shear modulus
κ	Poisson's coefficient function
j	Imaginary unit
A, B, C, E, F	CJP model coefficients
$z = x + jy$	Complex variable
K_F, K_R, K_S	CJP model stress intensity factors
T_x, T_y	Non-singular stresses
u_e, v_e	Experimental displacement field
$x_{SD}^{min}, x_{SD}^{max}, y_{SD}^{min}, y_{SD}^{max}$	Search domain bounds
$\Delta x, \Delta y$	Crack tip coordinates
u_0, v_0, R_x, R_y	Rigid body motion coefficients
$\Re$	Complex number real part
$\Im$	Complex number imaginary part
K_N	Nominal stress intensity factor
a	Crack length
W	Specimen width
t	Specimen thickness
d	Euclidean distance between crack tip locations
t_{GA}	GA optimisation time
t_{IP}	IP optimisation time
t_T	Total optimisation time

formulation of the model creates a nonlinear problem. Several techniques can be found in published literature that solve a similar problem. For instance, Yoneyama et al [18] simultaneously determined mixed-mode stress intensity factors, crack-tip location, and higher-order terms in the series expansion of displacement fields and rigid-body displacement components using a nonlinear least squares approach based on the Newton–Raphson method [7]. They used the Newton-Raphson method to solve the problem and the initial solution used values of singularity parameters provided by empirical correlations. Zanganeh et al [19] used the DIC displacement field around a crack tip in work to compare the influence of various methods that they used to locate the crack-tip position, on the values they found for stress intensity factors. They compared two constrained Newton type methods: the trust-region reflective Newton method and the quasi-Newton method; an unconstrained direct search method: the Nelder–Mead Simplex method; a constrained genetic algorithm; and a constrained Pattern Search (PS) method. They showed that the Newton type methods were less accurate compared with the direct search methods studied, while the PS technique was found to be the most accurate. Furthermore, the PS technique was found to be about twice as fast as the Simplex method and ten times faster than a Genetic Algorithm for the same computing hardware and the same input data. Yang et al [20] used the Levenberg-Marquardt algorithm [21] taking as the initial solution those values previously determined through linear fitting.

However, these techniques are not optimum for fitting experimental data to the mathematical formulation of the CJP model due to several factors. The CJP model describes the singularity field in terms of five coefficients that are related to the effect on the global elastic field of the plastic enclave that surrounds the crack. Empirical correlations for these coefficients are not available in the literature and finding suitable initial values for them is not straightforward. Equally, estimating an initial solution by linear fitting is not suitable in the case of the CJP model. A sensitivity analysis to evaluate how the crack tip position could affect the SIF calculation and the quality of the fit was performed by Vasco-Olmo [17] by analysing simulated horizontal and vertical displacement fields. An error of a few pixels in crack tip location was therefore intentionally introduced, leading to the conclusion that the CJP model was rather sensitive to variations in the crack tip position, particularly in the case of the x-coordinate. However, variations in the y-coordinate of the crack tip were not so critical. The ability of the CJP model in accurately characterising the plastic zone and plasticity-induced shielding has been widely demonstrated [16,22–25], and it would be useful to develop a technique that could be easily automated, and that allows an accurate crack tip position and corresponding characterisation of the crack tip fields to be obtained.

This work therefore describes a robust, fast, geometry-independent technique, developed for the CJP model, that calculates crack tip singularity parameters and accurately locates the crack tip position, and that is capable of automation. The proposed methodology addresses the problem through an optimisation approach that combines a stochastically chosen initial solution obtained via a genetic algorithm, with a deterministic gradient-based interior point method. The combination of these two methods provides a powerful tool for accurate calculation of the crack tip singularity parameters (SIFs and T-stresses), as well as correctly determining the crack tip location. The genetic algorithm (GA) generates a well-conditioned initial solution for the nonlinear problem while the interior point (IP) algorithm significantly reduces the high computational time usually associated with GA solutions. A further benefit is that the absence of the requirement for an initial problem solution allows automating the process, which is very useful in the

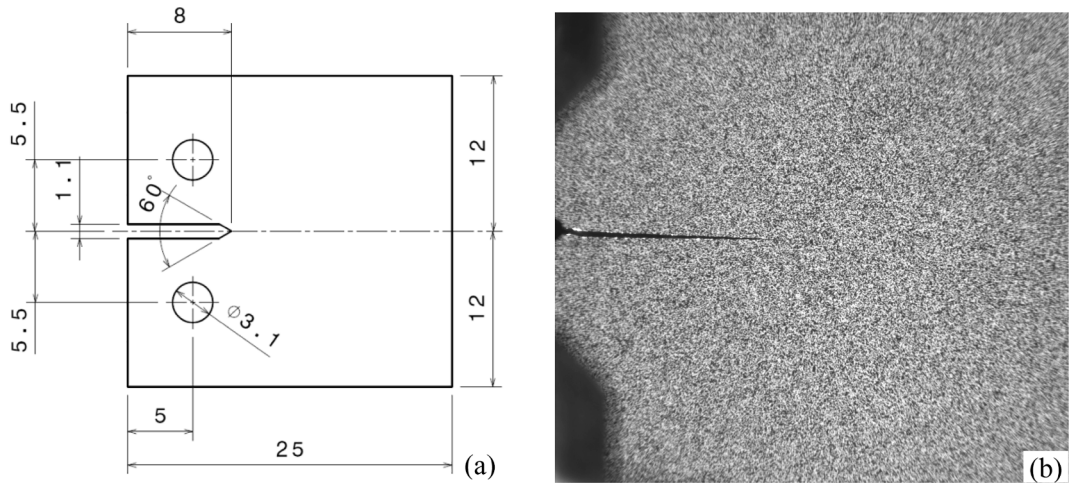

Fig. 1. (a) Dimensions of the CT specimen (mm). (b) Speckle pattern sprayed onto the specimen surface for the DIC work.

Table 1
Chemical composition of commercially pure titanium Grade 2.

Element (wt %)	Fe	C	N	O	H	Ti
Specification	< 0.20	≤ 0.08	≤ 0.05	≤ 0.20	≤ 0.015	Balance
Specimen	0.10	0.01	<0.01	0.12	0.002	Balance

Table 2
Mechanical properties for the commercially pure titanium Grade 2 tested in this work.

Parameter	E (GPa)	UTS (MPa)	σ_{ys} (MPa)	ε_f (%)	ν
Value	105	448	390	20	0.33

analysis of crack tip fields.

2. Theoretical fundamentals

2.1. Mathematical description of crack tip fields in the CJP model

The CJP model [11–13] is a linear elastic mathematical model for describing crack-tip fields based on Muskhelishvili's complex potentials [8,9]. However, the important innovation in the model is that the elastic analysis explicitly incorporates possible influences of the plastic enclave that surrounds the crack on the global elastic field. It does this by solving for any effects of plasticity-induced wake contact [26] and the necessary compatibility-induced strains at the elastic–plastic boundary. These latter strains arise from the change in Poisson's ratio between the elastic and plastic regions. The crack tip displacement fields defined by the CJP model, assuming that $D = -E$, i.e. asymptotic behaviour of the stress along crack flanks, is given by equation (1) [13]:

$$2G(u+vj) = \kappa\left[-2(B+2E)z^{\frac{1}{2}} + 4Ez^{\frac{1}{2}} - 2Ez^{\frac{1}{2}}\ln(z) - \frac{C-F}{4}z\right] - z\left[-(B+2E)\overline{z}^{\frac{-1}{2}} - E\overline{z}^{\frac{-1}{2}}\overline{\ln(z)} - \frac{C-F}{4}\right] - \left[A\overline{z}^{\frac{1}{2}} + E\overline{z}^{\frac{1}{2}}\overline{\ln(z)} - 2E\overline{z}^{\frac{1}{2}} + \frac{C+F}{2}\overline{z}\right] \quad (1)$$

In this equation, G is shear modulus, u and v are the horizontal and vertical field components, respectively, j is $\sqrt{-1}$, κ is a function of Poisson's coefficient that depends on whether the crack experiences plane stress or plain strain conditions [13], z is a complex variable ($x + jy$) and A, B, C, E and F are the coefficients governing the crack tip singularity. The overbar denotes the complex conjugate and ln denotes the natural logarithm operator. Coefficients A, B and E are related to the three stress intensity factors defined by the model. The opening mode stress intensity factor that drives the crack forwards, denoted by K_F, a retardation stress intensity factor that acts against the crack in its plane, denoted by K_R and a shear-induced stress intensity factor denoted by K_S. C and F are the coefficients that determine non-singular stresses along the crack growth (x) and crack opening directions (y), respectively. These crack tip parameters are given by equations (2) to (6) [13].

$$K_F = \sqrt{\frac{\pi}{2}}(A - 3B - 8E) \quad (2)$$

$$K_R = -(2\pi)^{\frac{3}{2}}E \quad (3)$$

$$K_S = \sqrt{\frac{\pi}{2}}(A + B) \quad (4)$$

$$T_x = -C \quad (5)$$

$$T_y = -F \quad (6)$$

2.2. Optimisation algorithms for nonlinear multidimensional problems

2.2.1. Genetic algorithms

Genetic algorithms (GA) [22] as used in mathematical optimisation

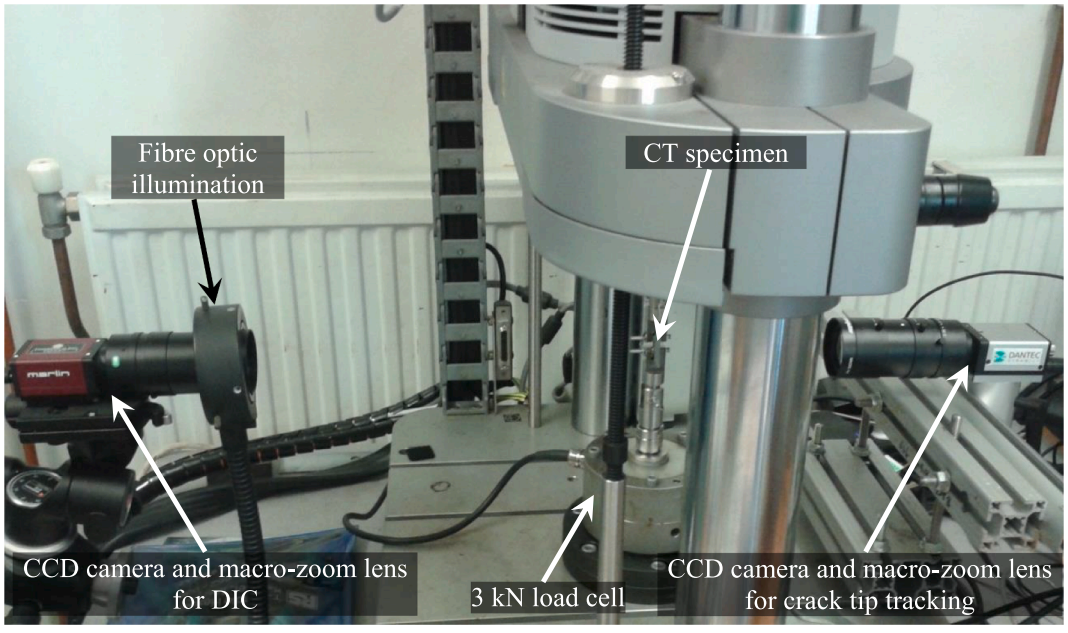

Fig. 2. Experimental set-up used in the fatigue testing and for data acquisition.

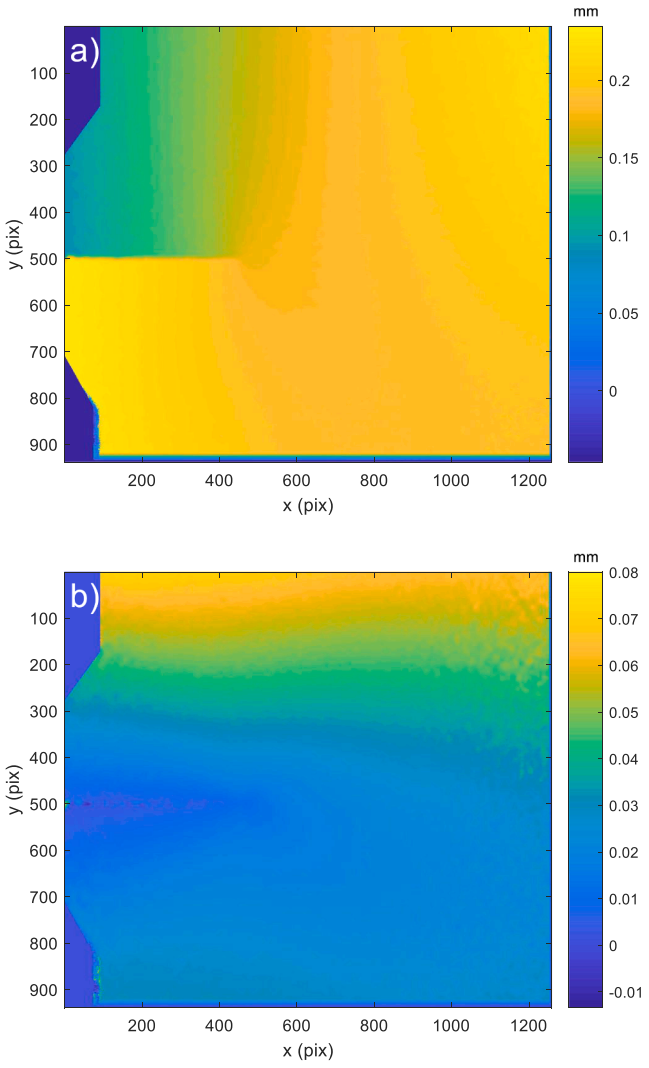

Fig. 3. (a) Vertical and (b) horizontal displacement maps measured with DIC for a 9.40 mm crack at a load of 750 N.

are heuristic, direct search, constrained or unconstrained, and zero order methods based on concepts derived from Darwinian species evolution theory. In a general way, GAs operate as follows. An initial solution population is created stochastically and these "individuals" are evaluated via an objective or fitness function to determine their 'survival' value. According to evolutionary theory, the fittest progenitors must produce the fittest subsequent generation. Thus, the best individuals in the population, according to their fitness value, are selected to create a new and improved generation by replacing the least fit individuals. a better solution is then generated by combining the best progenitors through crossover and mutation operations. This process is repeated through subsequent generations until a solution is found that satisfies the fitness function to the desired accuracy. In mathematical optimisation, GAs are employing in highly nonlinear problems to find global minima. This kind of algorithm is computationally expensive since they usually require a large number of iterations. However, these methods are the only ones that can ensure that a global minimum solution is found. Their advantage is that they do not require accurate initial solutions due to their stochastic and evolutionary nature, compared with other deterministic methods where a well-chosen initial solution is required to achieve a global minimum. GA techniques are often used in conjunction with a second technique to find local minima; this is useful when several global minima have similar values.

2.2.2. *Interior point algorithms*

Interior point (IP) algorithms for nonlinear optimisation [23–27],

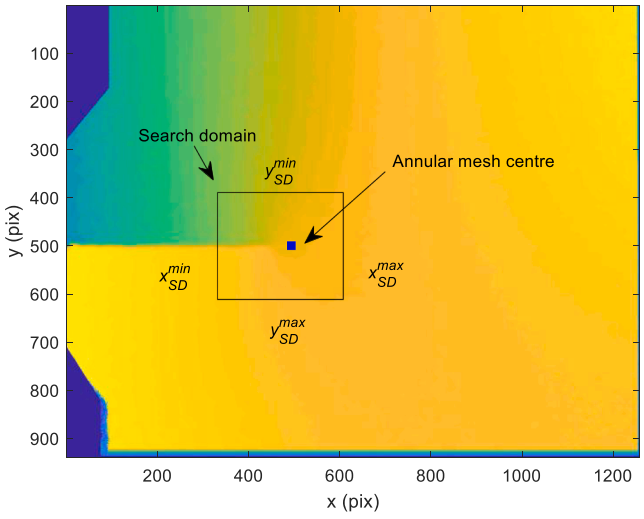

Fig. 5. Search domain in the vertical component of the displacement field.

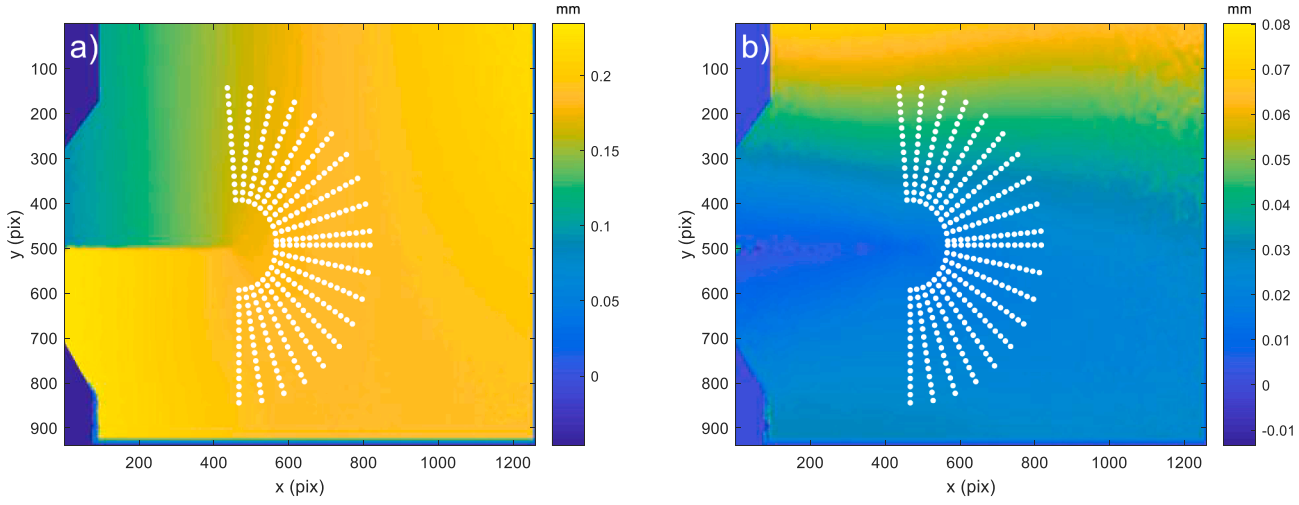

Fig. 4. Annular mesh superimposed on a) vertical and b) horizontal displacement maps for a crack length of 9.4 mm at maximum load.

also known as barrier methods, are deterministic, gradient-based methods for constrained optimisation problems. These methods are considered the most suitable for problems involving large-scale nonlinear optimisation [28]. IP methods were conceived as alternatives to the Dantzig-Simplex method [29] for solving large linear problems. They provide a fast optimisation if the initial solution is well conditioned. The IP algorithm transforms inequality constraints via a barrier logarithmic term that is added to the objective function to include deleted inequality constraints. The problem therefore remains an equality constrained problem whose solution is simpler. Hence, by applying the first order optimality conditions [30] to the barrier problem, together with equality constraints, allows a nonlinear equation system to be obtained which can be addressed using Newton's method. Further detail about how each sub-problem is addressed are given in section 4.1. Additional information about the IP algorithm scheme, as well as the relaxation factors employed in this work, can be found in the paper published by Waltz et al [27].

2.2.3. Hybrid approach: Combining heuristic and deterministic methods

As already mentioned, the most effective way of solving large scale, highly nonlinear optimisation problems, where an initial well-conditioned solution is difficult to find, is via the combination of a genetic algorithm with a second optimisation technique. A hybrid approach is developed in this work that initiates the fitting process with a GA, to avoid the necessity of including an initial well-conditioned solution. After a certain number of iterations, when the GA solution is relatively close to the global minimum, the IP technique is incorporated which uses as its initial solution the one provided by the GA. This approach avoids the disadvantages of the two individual optimisation techniques, as the GA starts with ill-conditioned data and the computation time is reduced by the IP method.

3. Experimental work

A 1 mm thick sheet of commercially pure Grade 2 titanium was used to manufacture a compact tension (CT) specimen (with the geometry shown in Fig. 1a) that was tested in constant amplitude loading at a stress ratio value of 0.6 with a maximum load of 750 N. Table 1 shows the specified chemical composition for Grade 2 titanium, along with the data measured from the specimen sheet; mechanical property data are given in Table 2.

Both surfaces of the specimen were prepared to enable simultaneous measurements of the displacement fields via digital image correlation (DIC) on one side and crack length via a zoom charge-coupled device (CCD) camera on the other. The side of the specimens for the DIC measurements was sprayed with a random black speckle pattern (shown in Fig. 1b) using an airbrush over a white background. In addition, the opposite side of the specimen was ground and polished to enable tracking the crack tip position using a second 1 Mpixel charge-coupled device (CCD) camera (Dantec Dynamics) fitted with a macro-zoom lens (Edmund Optics, model MLH-10X EO) (Fig. 2). In addition, the crack length measurements were used during fatigue testing in order to provide uniform crack increments between DIC measurements of the crack tip displacement field.

Fatigue testing used an Electropuls E3000 electrodynamic machine (Fig. 2) at a loading frequency of 10 Hz. DIC measurements were made with a 1 Mpixel CCD camera (Allied Vision Technology, model Marlin F-146B/C) mounted perpendicular to the specimen surface. The camera system used a macro-zoom lens, similar to the one used in crack tip tracking, to image crack propagation with a resolution of 13.7 μm/pixel (field of view of 17.3 × 13 mm). A fibre optic light ring placed around the macro zoom lens provided illumination of the specimen surface (also shown in Fig. 2).

During fatigue testing, the cyclic loading was periodically paused to acquire a sequence of crack tip displacement images at uniform load increments of 25 N, representing 30 images for both the loading and unloading half-cycles. Image processing used the Vic-2D program from Correlated Solutions with 25 pixels as the subset size and a step value of 1 pixel, to give the maximum resolution for the displacement maps. Fig. 3 shows an example of the horizontal and vertical displacement fields for a crack length of 9.40 mm and a load of 750 N.

4. Data processing

4.1. Displacement data and optimisation procedure

The u_e and v_e data used in the fitting process was obtained from the displacement fields measured ahead of the crack tip outside the high strain plastic zone near the crack tip. In order to do this, an annular data collection region was defined (Fig. 4) via an inner and outer radius, the sweep angle and the mesh centre. The inner radius was calculated by estimating the plastic zone size, so to avoid including the zone of crack tip plasticity. The estimation method described by Vasco-Olmo et al [31] in experimental work on estimation of both size and shape of the plastic zone from displacement field analysis was used for this. The outer radius of the annulus must capture the full crack tip singularity zone. This was ensured using to the criterion described by Vasco-Olmo et al [32], based on the observation of the vertical displacement maps (Fig. 3a), where the singularity dominance zone is recognised via the displacement contours being straight and perpendicular to the crack. As the dominance ceased, these contours start to tilt (see Fig. 3a). Nonetheless, the chosen outer radius size is not a sensitive parameter and an overestimation of the singularity zone value does not significantly affect the results. The mesh sweep angle was chosen as 180 degrees.

If the crack tip location had not been included in the optimization problem, the selected position of the mesh centre would be a critical parameter, as crack tip models generally consider that the crack tip corresponds with the coordinate origin. In the current approach, the mesh centre was simply chosen so as to place the mesh approximately in the singularity zone. During the fitting process, the spatial position of the crack tip changes until an optimum solution is found.

A search domain was defined that enclosed the crack tip location in order to reduce the GA computational time (Fig. 5). The exact crack tip location is not easily determined from displacement field maps; however, a confidence region can be easily established simply from observation of the displacement maps. The search domain was therefore defined by the centre of the annular mesh and an offset value as shown in Fig. 5. A sensitivity analysis of the search domain size was made that demonstrated that increasing its size increased computation times without modifying the computed singularity parameters or the crack tip location. A size of around 10% of the crack length was eventually chosen to give reasonable computation times and allow analysing the crack path during the optimisation process. The inclusion of the search domain into the optimisation problem adds two constraints (upper and lower bounds for x and y) that enclose the crack tip coordinates.

Once fitting data had been extracted from the displacement field maps and the constraints were defined, the optimisation problem was formulated as shown in equation (7):

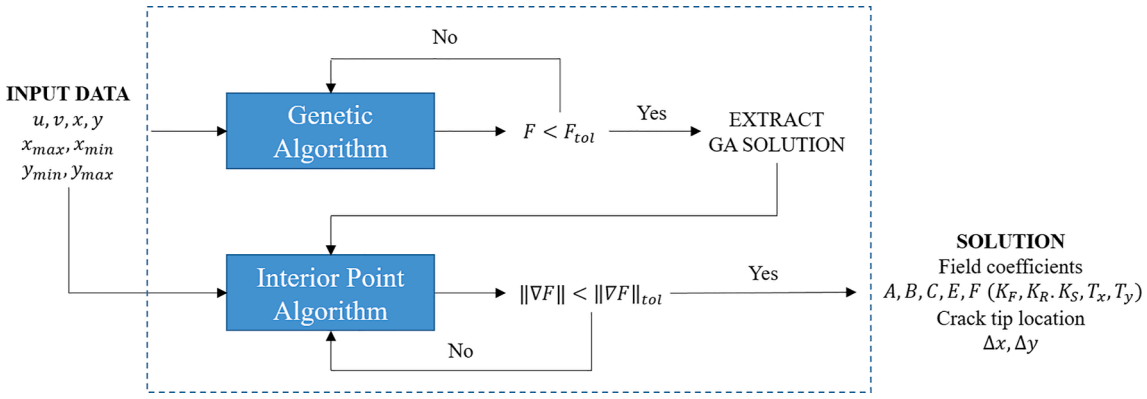

Fig. 6. Hybrid optimisation scheme.

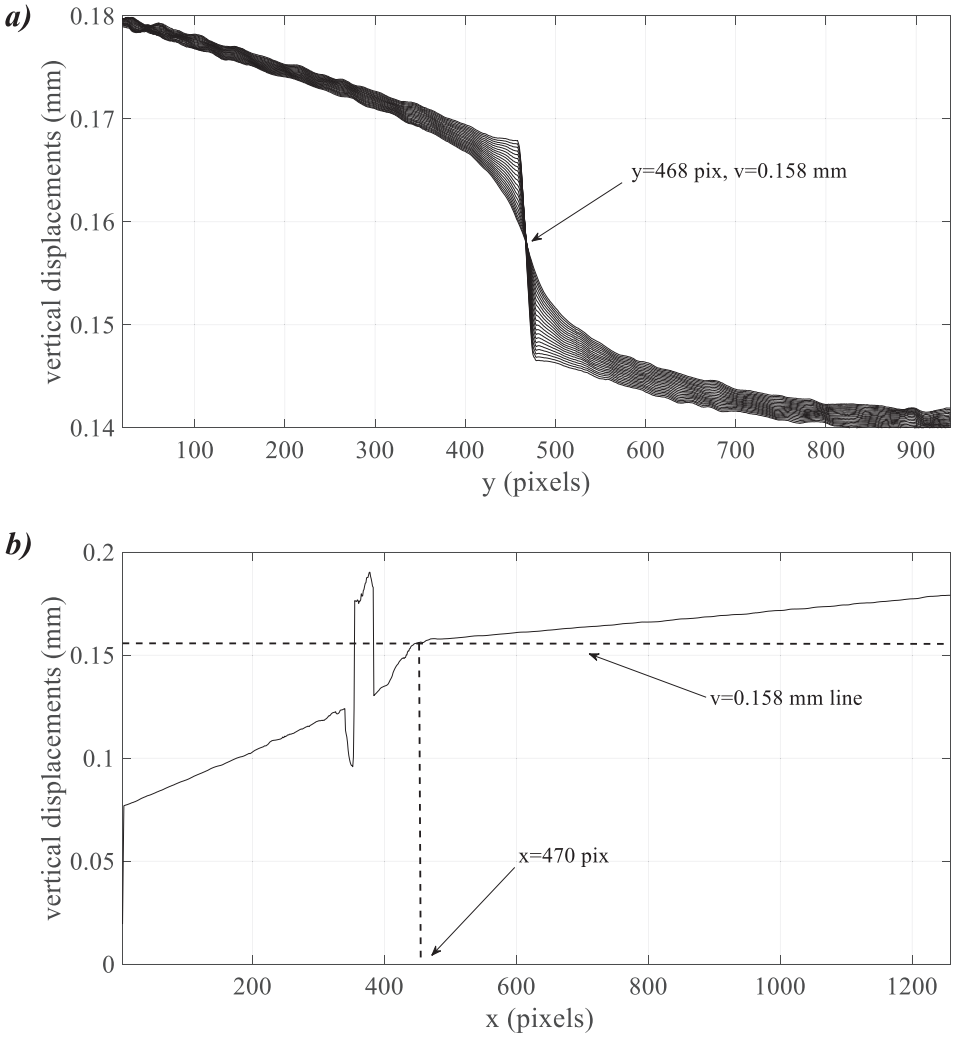

Fig. 7. Plots showing the methodology used to identify the position of the crack tip in the y (a) and $\times$ (b) directions.

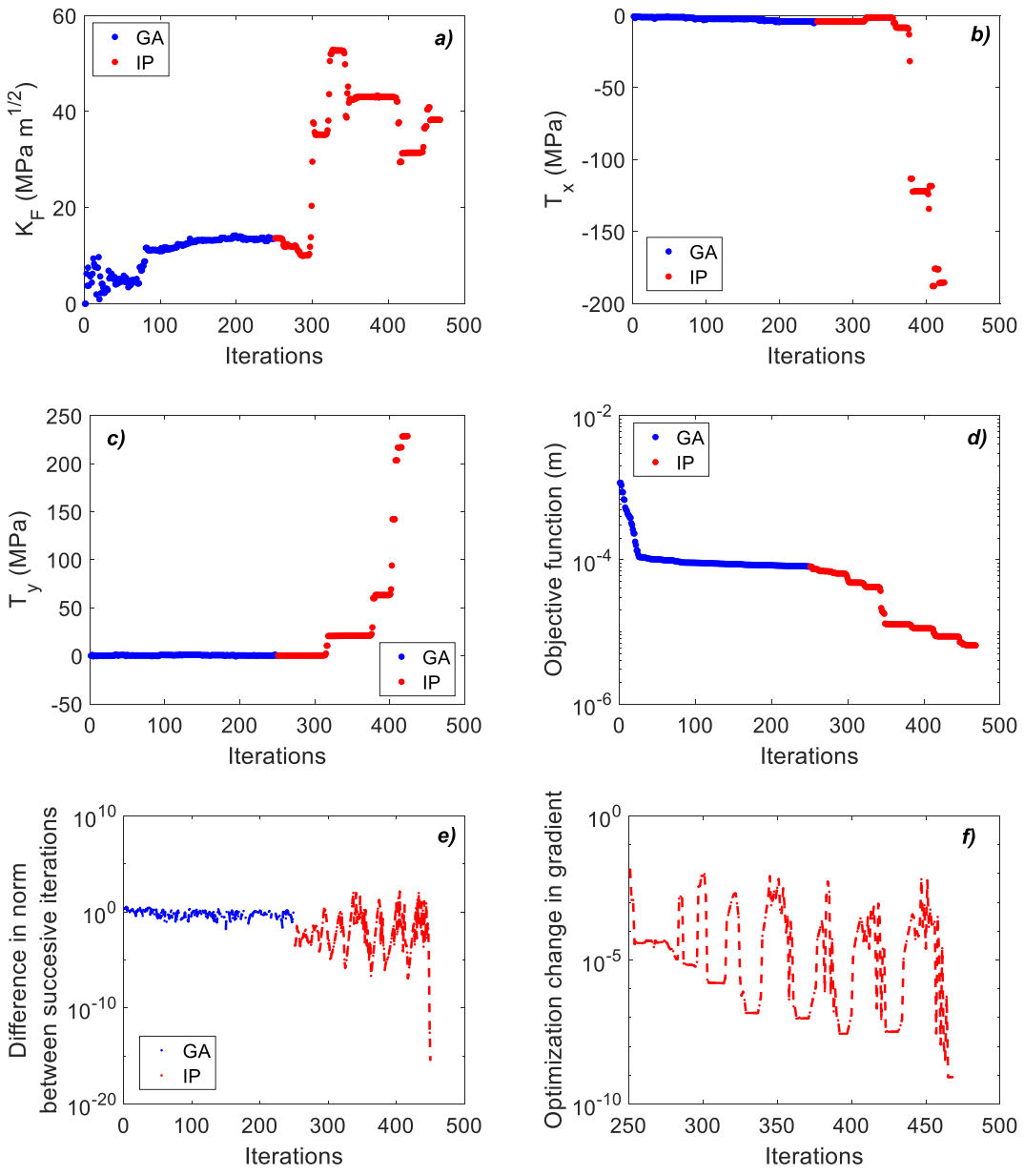

Fig. 8. The changes in specific parameters observed during the optimisation process for a crack length of 7.75 mm. a) CJP opening mode SIF $\boldsymbol{K_F}$, b) and c) Non-singular stresses $\boldsymbol{T_x}$ and $\boldsymbol{T_y}$, d) Objective function e) Difference in norm between successive iterations and f) Optimisation change in gradient (only computed for the gradient-based method).

$$\min_{\substack{A,B,C,E,F\\ \Delta x,\Delta y,u_0,v_0\\ R_x,R_y}} \|2G(u_e+v_e j)-\kappa\left[-2(B+2E)(z-\Delta x-j\Delta y)^{\frac{1}{2}}+4E(z-\Delta x-j\Delta y)^{\frac{1}{2}}-2E(z-\Delta x-j\Delta y)^{\frac{1}{2}}\ln(z-\Delta x-j\Delta y)-\frac{C-F}{4}(z-\Delta x-j\Delta y)\right]$$
$$+(z-\Delta x-j\Delta y)\left[-(B+2E)\overline{(z-\Delta x-j\Delta y)}^{\frac{-1}{2}}-E\overline{(z-\Delta x-j\Delta y)}^{\frac{-1}{2}}\ln(z-\Delta x-j\Delta y)-\frac{C-F}{4}\right]+\left[A\overline{(z-\Delta x-j\Delta y)}^{\frac{1}{2}}+E\overline{(z-\Delta x-j\Delta y)}^{\frac{1}{2}}\ln(z-\Delta x-j\Delta y)\right.$$
$$\left.-2E\overline{(z-\Delta x-j\Delta y)}^{\frac{1}{2}}+\frac{C+F}{2}\overline{(z-\Delta x-j\Delta y)}\right]+2G\big(-u_0-v_0 j-R_x\Im(z-\Delta x-j\Delta y)+jR_y\Re(z-\Delta x-j\Delta y)\big)\|_2 \quad (7)$$

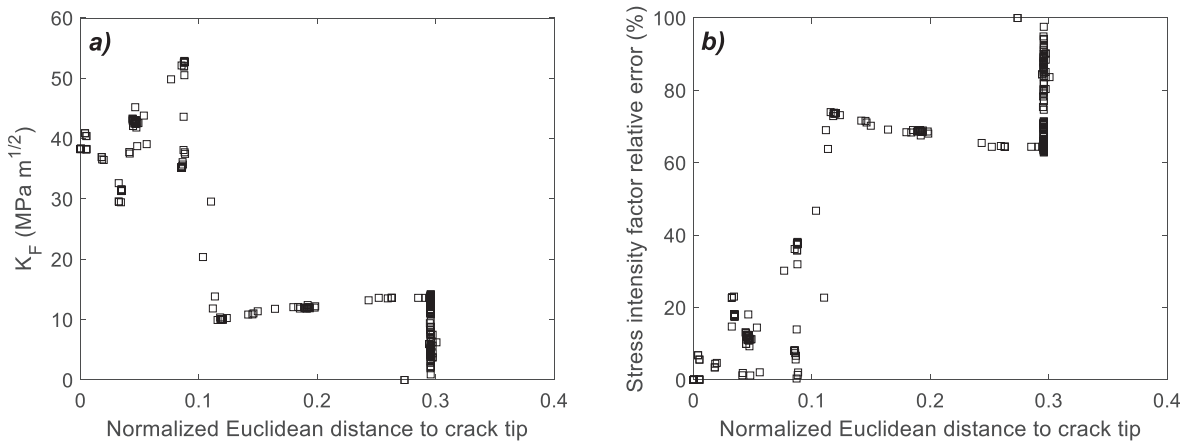

Fig. 9. Variation in opening mode SIF with the normalised Euclidean distance to the crack tip for a crack length of 7.75 mm. Crack tip distance normalised by crack length. a) $\boldsymbol{K_F}$ and b) Relative error in terms of.$\boldsymbol{K_F}$

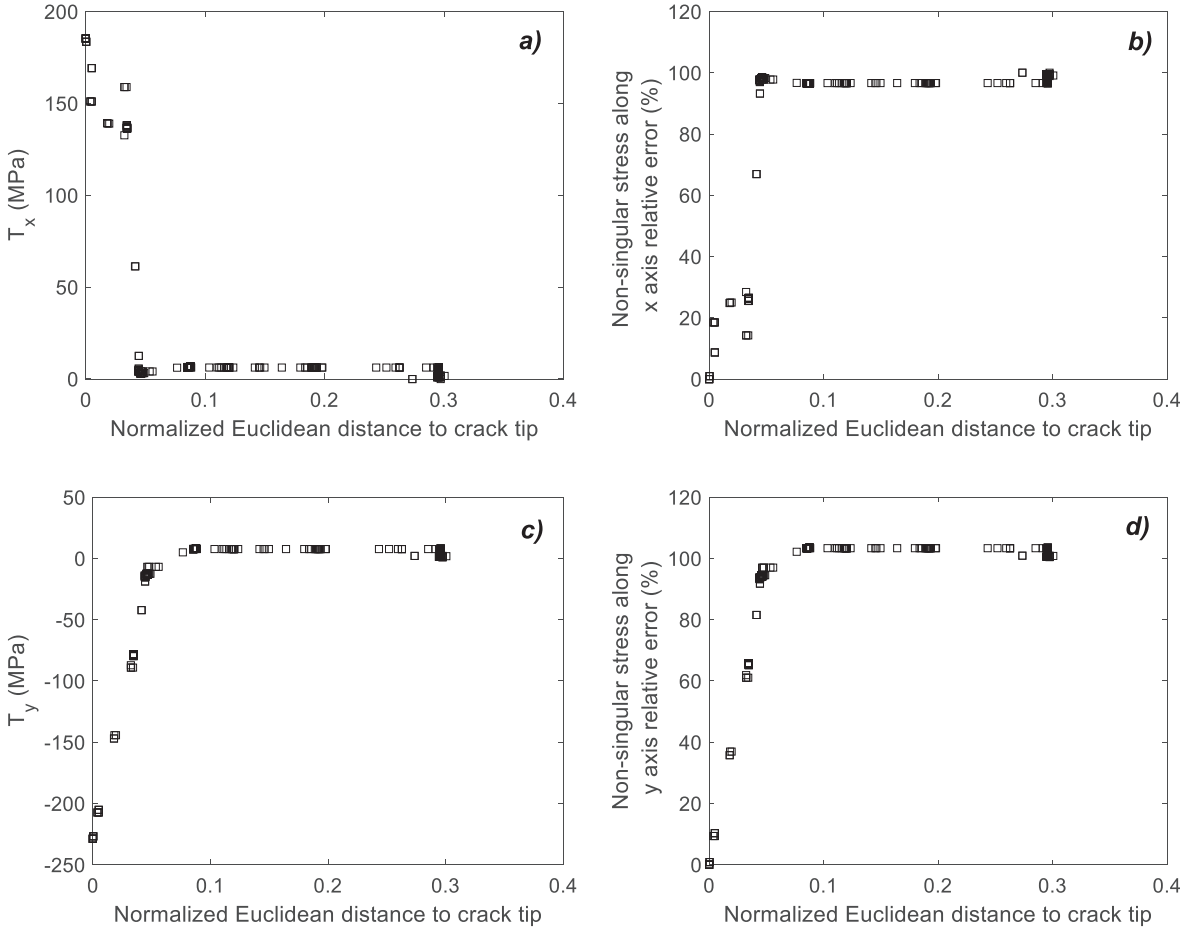

Fig. 10. Variation of non-singular stresses with the normalised Euclidean distance to the crack tip for a crack length of 7.75 mm. Crack tip distance normalised by crack length. a)$\boldsymbol{T_x}$, b) $\boldsymbol{T_x}$ relative error, c) $\boldsymbol{T_y}$ and d) $\boldsymbol{T_y}$ relative error.

$s.t. x_{SD}^{min} < \Delta x < x_{SD}^{max}$

$y_{SD}^{min} < \Delta y < y_{SD}^{max}$

$A, B, C, E, F, \Delta x, \Delta y, u_0, v_0, R_x, R_y notsignconstrained$

In this equation, u_e and v_e are the displacement field components, Δx and Δy are the distances between crack tip position and map origin,u_0, v_0, R_x and R_y are the in-plane rigid body motion coefficients (u_0 and v_0 are horizontal and vertical rigid body translations and $R_x = R_y$ the displacement due to in xy plane rigid body rotation) and x_{SD}^{max}, x_{SD}^{min}, y_{SD}^{max}, y_{SD}^{min} are the bounds of the search domain. Double vertical bars denote the Euclidean norm of the expression. Operator $\Re$ denotes the real part of a complex number and operator $\Im$ denotes the imaginary part of a com-

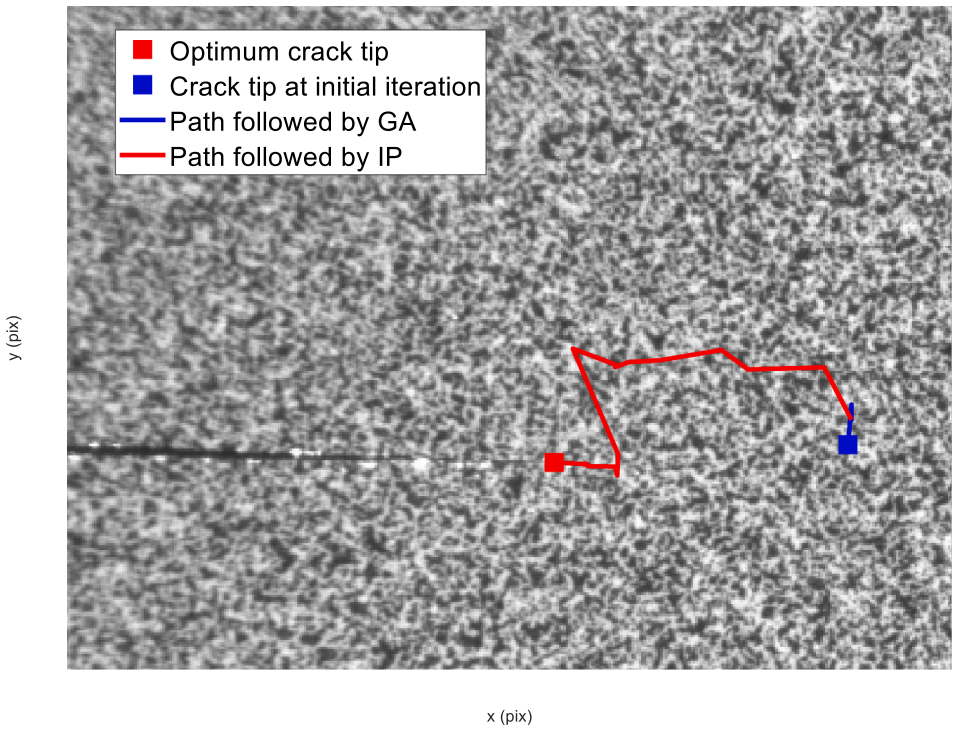

Fig. 11. Illustration of the final optimum crack tip position (red square), the crack tip position at the first iteration (blue square), and paths followed by the optimization algorithms (blue GA and red IP) superimposed on the speckle image. Crack length of 7.75 mm.

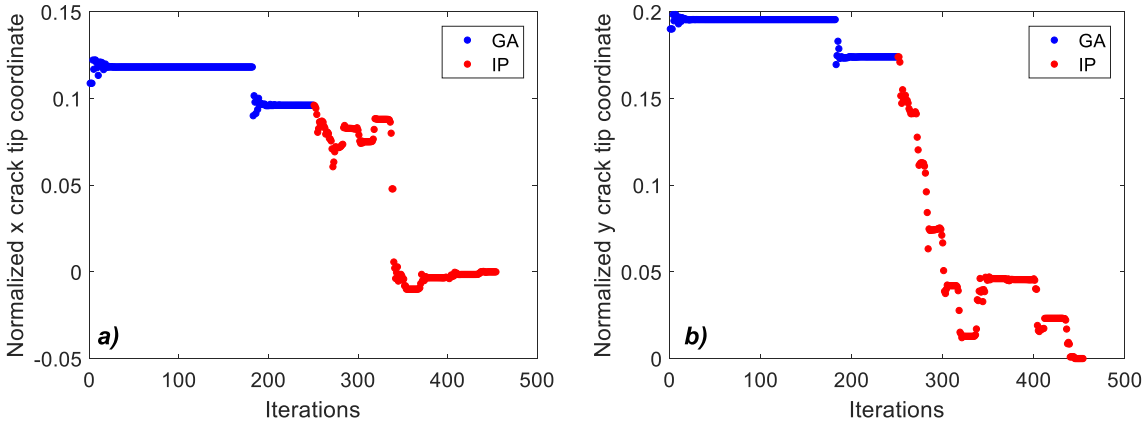

Fig. 12. Changes in the *x* and *y* crack tip coordinates during the iterative process, normalised as the ratio of the distance between their × and y distances and the optimum crack tip position divided by the crack length A value of zero corresponds with the normalised optimum crack tip position during the optimisation process. a) *x*-coordinate and b) *y*-coordinate.

plex number.

The optimisation problem defined in equation (7) remains highly nonlinear and has a large number of variables to optimise. The initial solution chosen for running the algorithm is therefore a critical variable in the fitting problem. A well-conditioned initial solution cannot be easily found since some CJP coefficients are related to nonlinear effects on the elastic field and hence there are no correlations available to estimate these parameters a priori. To avoid defining an initial solution a GA was used to initialise the optimisation problem. When the solution provided by the GA is close to an optimum (determined by checking relative error between theoretical and experimental fields), the IP algorithm starts by taking its initial solution to be the last solution iteration generated by the GA. In this way, potential errors arising from incorrect choice of initial solutions are avoided and computational times are considerably reduced. A schematic of this hybrid approach is shown in Fig. 6.

Fig. 6 illustrates a clear advantage of this approach, in that it is easily automated since only the displacement fields are necessary to calculate the crack tip parameters. In the GA part of the optimisation process, the objective function value was chosen as criterion for stopping further iterations, whilst during the IP optimisation the norm of the objective function gradient was chosen as the criterion for terminating the process. It was observed that in order to achieve a well-conditioned GA solution that is then used to initiate the IP algorithm, the relative value of the error function (quotient between error function and theoretical CJP displacement field) had to be between 15% and 20%. In the GA process a population of 250 individuals was defined and the initial population was generated from a uniform statistical distribution by defining two upper and lower symmetrically bounds. For unconstrained variables a [-10, 10] range was chosen and for constrained variables their defined bounds were used. At the end of each iteration, individuals were sorted using their rank in place of their fitness value since closer

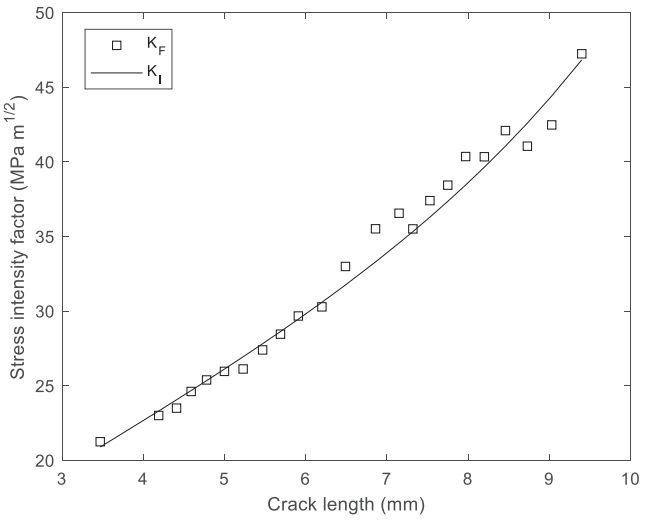

Fig. 13. Experimentally determined CJP driving force, K_F, and standard Mode I stress intensity factor versus crack length at maximum load.

fitness values between individuals can lead to problems during the sorting stage. The fraction of surviving individuals was defined using a 5% elitism level. Separate from the elite individuals, 70% percent of the next generation of data was generated by a crossover technique that used a linear combination between weighted progenitor data according to their fitness values. Finally, mutation was allowed in order to keep the last convergence direction compliant with the defined constraints. In this work, the IP algorithm used a quasi-Newton and trust-region approach [25]. The objective gradient was computed by finite difference using the central derivative to reduce discretisation errors and improve the accuracy of the results. The Hessian matrix was computed using the Broyden-Fletcher-Goldfarb-Shanno (BFGS) algorithm [33–35]. Using a full-Newton approach, convergence could be achieved faster than with a quasi-Newton approach. However, the inclusion of analytical derivatives (either first and second order, or first order and second order by finite difference) into the algorithm increased the computational time and cost. It was noted that the conjugate gradient trust-region approach for solving each sub-problem was very useful in achieving convergence to a global minimum. In contrast, if a line search approach was used, the algorithm could stall in finding a local minimum.

4.2. Results verification

To demonstrate that the proposed methodology provided an accurate calculation of the crack tip location as well as the stress intensity factors, its results were compared with those obtained using the following two procedures.

4.2.1. Crack tip location from the analysis of vertical displacement maps

In this technique, the $\times$ and y coordinates of the crack tip were obtained as follows. Firstly, the y-coordinate is found as the intersection point observed when a set of vertical displacement profiles, plotted perpendicularly to the crack path, cross the crack plane. This convergent behaviour of the profiles at a point on the crack plane can be clearly seen in Fig. 7a. The vertical displacement value (v = 0.158 mm) corresponding to this intersection point is indicated in Fig. 7a because it is used to find the crack tip position in the x-direction (Fig. 7b).

Fig. 7b plots a vertical displacement profile in the x-direction parallel to the crack path and allows identification of the x-coordinate of the crack tip as that point on the displacement profile that has the same value for the vertical displacement identified for the y-coordinate of the crack tip. The $\times$ and y coordinates of the crack tip identified from this procedure were 470 pixels and 468 pixels, respectively, taking the upper left corner of the displacement map (Fig. 3b) as the coordinate origin. This methodology was then applied for all the crack lengths measured during the fatigue testing.

4.2.2. Standard functions for determination of nominal SIF

The second comparison technique used the standard elastic compliance function for a CT specimen provided by the ASTM [36], which is given in equation (8):

$$K_I = \frac{P}{t\sqrt{W}} \frac{2+\frac{a}{W}}{\left(1-\frac{a}{W}\right)^{\frac{3}{2}}} \left[0.886+4.64\left(\frac{a}{W}\right)-13.32\left(\frac{a}{W}\right)^2+14.72\left(\frac{a}{W}\right)^3-5.6\left(\frac{a}{W}\right)^4\right] \quad (8)$$

Table 3
Crack tip locations and opening mode SIFs for different crack lengths. Comparison and differences.

	Optimised Technique		Vertical Displacement Technique							
a	Δx	Δy	Δx	Δy	d	d	d/a	K_F	K_I	SIFs error
mm	pix	pix	pix	Pix	pix	μm	(%)	MPa $m^{1/2}$	MPa $m^{1/2}$	(%)
3.47	56	486	60	482	5.66	73.0	2.24	21.25	20.89	1.71
4.19	107	484	100	481	7.62	99.0	2.48	23.01	23.31	1.29
4.41	117	481	108	481	9.00	117	2.65	23.50	24.06	2.32
4.59	129	481	120	481	9.00	117	2.54	24.62	24.68	0.25
4.78	138	481	130	480	8.06	104	2.17	25.39	25.34	0.19
5.00	154	481	156	480	2.24	29.0	0.52	25.96	26.12	0.59
5.23	168	481	163	477	6.40	83.2	1.49	26.12	26.94	3.03
5.47	188	478	183	477	5.10	66.2	1.18	27.40	27.81	1.49
5.69	193	478	192	479	1.41	18.3	0.22	28.46	28.63	0.61
5.91	212	478	209	479	3.16	41.1	0.65	29.67	29.46	0.71
6.20	244	479	240	477	4.47	58.1	0.83	30.28	30.59	1.00
6.49	267	477	265	477	2.00	26.0	0.40	32.99	31.75	3.90
6.86	288	477	285	475	3.61	46.7	0.75	35.51	33.29	6.67
7.15	308	477	307	475	2.24	29.0	0.36	36.56	34.56	5.79
7.32	321	476	323	474	2.83	36.7	0.53	35.51	35.32	0.52
7.53	336	476	340	475	4.12	53.6	0.69	37.40	36.30	3.04
7.75	350	475	346	474	4.12	53.6	0.67	38.44	37.35	2.90
7.97	367	475	370	473	3.61	46.8	0.65	40.36	38.45	4.96
8.20	385	473	382	474	3.16	41.1	0.47	40.34	39.64	1.77
8.46	400	474	400	474	0.00	0.00	0.00	42.10	41.05	2.54
8.73	424	472	425	474	2.24	29.0	0.29	41.05	42.60	3.63
9.03	447	472	443	473	4.12	53.6	0.57	42.47	44.41	4.37
9.4	470	471	470	470	1.00	13.0	0.13	47.24	46.83	0.87
	Average values				4.14	50				2.35

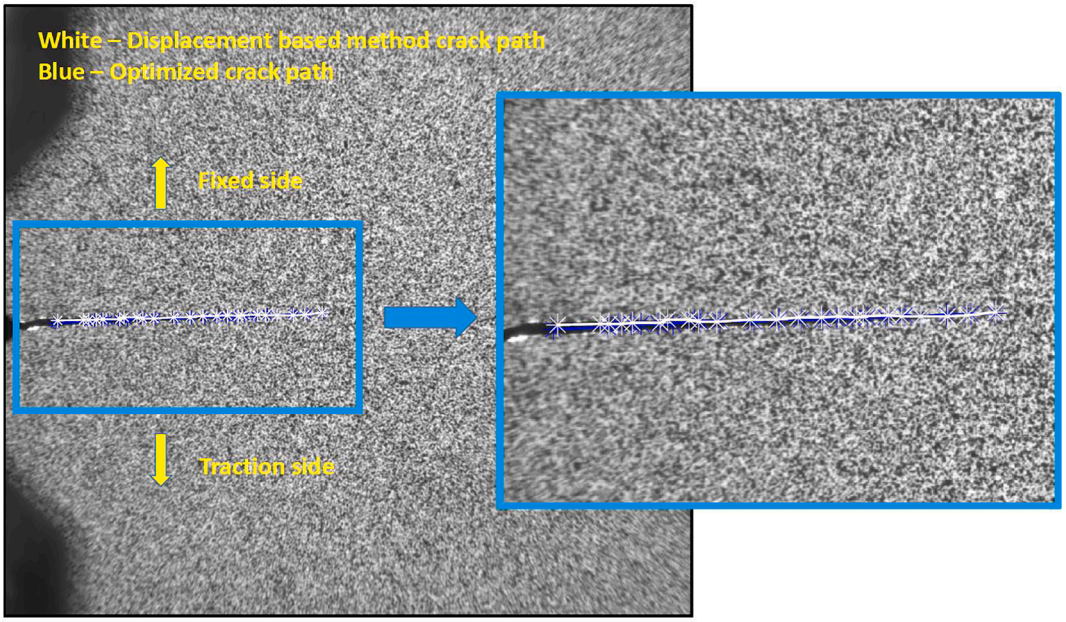

Fig. 14. Crack paths superimposed over the speckle image.

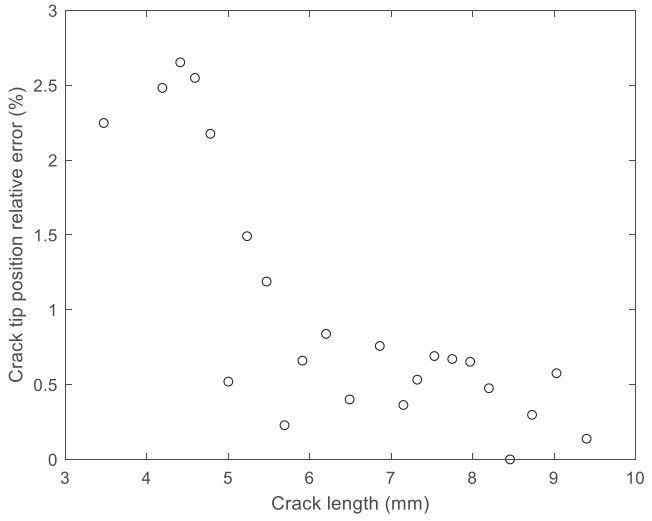

Fig. 15. Relative crack tip position difference between the hybrid optimisation and the displacement intersection methods.

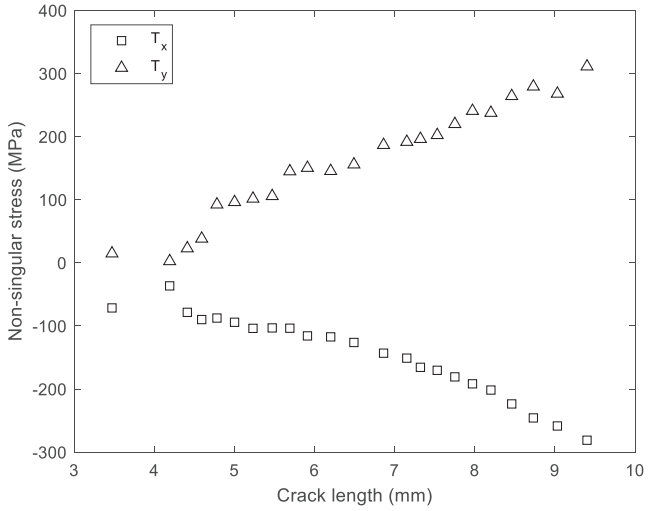

Fig. 16. Non-singular stresses along × and y axes in function of crack length.

where P is the applied load, t and W are the thickness and the width of the specimen, respectively.

5. Results and discussion

5.1. Convergence analysis

Convergence analysis results are presented for an illustrative crack length of 7.75 mm (a/W = 0.38), as typical of the results obtained for any other crack length. The changes in the various parameters observed during the optimisation process are shown in Fig. 8a (change in the opening stress intensity factor K_F), 8b (T-stress in the x-direction, T_x) and 8c (T-stress in the y-direction, T_y). Fig. 8f shows that the optimisation change in gradient while the algorithm is running reaches several successive local minima that are maintained over a number of iterations, before a clear global minimum is achieved. It clearly illustrates the complexity of the optimisation problem. At these local minima, the values found for the crack tip parameters (shown in Fig. 8a, 8b and 8c) do not represent the final solution. For example, in the case of the opening mode SIF K_F (Fig. 8a), either very low or very high values are found. Moreover, the change in the solution value between successive iterations is very significant, as indicated in the values of the non-singular T-stresses (Fig. 8b and 8c); as these parameters remain near zero until the optimisation approaches the global minimum at around 450 iterations. The objective function (Fig. 8d) shows two steep regions of decrease during the optimisation process. The initial decline is observed at the beginning of the GA optimisation over around 50 iterations. This decrease and its subsequent stabilisation are due to the GA generating a well-conditioned initial solution fairly quickly, but then experiencing some difficulty when the solution is refined. The GA can therefore provide a good solution in a short period of time but subsequently requires a substantial time or number of iterations in trying to achieve a global minimum. The second steep decline is observed during the IP optimisation at around 330 iterations, and this coincides with the zone where the crack tip parameters approach their final values. Fig. 8e

Table 4
Results for the CJP characterising parameters, crack tip location, error function and computation times for the various crack lengths.

a mm	K_F MPa $m^{1/2}$	K_R* MPa $m^{1/2}$	K_S MPa $m^{1/2}$	T_x MPa	T_y MPa	Δx pix	Δy pix	F m	t_{GA} s	t_{IP} s	t_T s
3.47	21.25	0.00	−3.26	−71.47	14.81	56	486	5.64E-09	54.65	5.46	60.11
4.19	23.01	0.00	−3.09	−36.55	2.56	107	484	7.91E-09	55.93	5.29	61.22
4.41	23.50	0.01	−4.03	−78.48	22.89	117	481	6.16E-09	57.13	3.92	61.05
4.59	24.62	0.00	−4.29	−89.93	38.26	129	481	8.34E-09	59.79	4.28	64.07
4.78	25.39	0.00	−1.57	−87.52	92.37	138	481	1.00E-08	56.02	3.25	59.27
5.00	25.96	−0.28	−2.45	−94.19	96.20	154	481	8.26E-09	54.96	6.63	61.59
5.23	26.12	−0.35	−2.96	−103.84	101.64	168	481	9.95E-09	53.89	4.96	58.85
5.47	27.40	0.00	−3.13	−103.17	105.71	188	478	1.38E-08	58.97	4.53	63.50
5.69	28.46	−0.24	−1.78	−103.63	144.95	193	478	2.71E-08	56.43	5.15	61.58
5.91	29.67	−0.07	−2.45	−115.79	150.43	212	478	2.04E-08	56.09	4.07	60.16
6.20	30.28	0.00	−3.18	−117.35	145.47	244	479	1.36E-08	57.65	3.47	61.12
6.49	32.99	−0.40	−3.61	−126.24	155.83	267	477	3.48E-08	53.47	3.87	57.34
6.86	35.51	−0.71	−3.59	−143.19	186.71	288	477	3.18E-08	53.55	3.86	57.41
7.15	36.56	−0.64	−4.18	−151.04	191.65	308	477	3.29E-08	54.28	5.97	60.25
7.32	35.51	−1.22	−5.12	−165.59	196.25	321	476	2.21E-08	57.33	4.11	61.44
7.53	37.40	−1.03	−5.26	−170.33	202.41	336	476	3.06E-08	57.91	3.55	61.46
7.75	38.44	−1.36	−5.38	−180.74	219.86	350	475	2.97E-08	53.75	5.55	59.30
7.97	40.36	−1.58	−5.49	−191.75	240.70	367	475	2.23E-08	58.34	4.15	62.49
8.20	40.34	−1.61	−6.32	−201.62	237.61	385	473	1.49E-08	56.01	4.05	60.06
8.46	42.10	−2.17	−6.73	−223.61	264.21	400	474	3.81E-08	52.74	5.20	57.94
8.73	41.05	−3.09	−7.65	−245.80	279.31	424	472	3.48E-08	55.39	5.71	61.10
9.03	42.47	−2.76	−9.32	−258.56	268.00	447	472	3.60E-08	54.81	5.95	60.76
9.40	47.24	−2.70	−9.16	−281.10	311.15	470	471	2.42E-08	58.42	4.43	62.85

* K_R values at the smaller crack lengths are not zero – they are low ($\sim 10^{-3}$) and positive.

shows the difference in the norm observed between successive iterations. This value changes from 10^{-1} to 10^{-16} when the global minimum is found. This observation, along with the associated steep decline in the optimisation change in gradient support the conclusion that an optimum value is achieved using this methodology.

The sensitivity of the crack tip parameters defined by the CJP model to the crack tip position is reflected in Fig. 9. The opening mode SIF K_F varies over a wide range of values (differences around 20%) even when the normalised distance to the computed crack tip location is<5% (0.05). Only when the normalised distance is lower than 2% (0.02) are accurate results obtained (differences lower than 5%). Similar trends are observed in the values of the non-singular T-stresses shown in Fig. 10, although this variable is even more sensitive to crack tip position, as for crack tip normalised distances of approximately to 1% (0.01) the relative error is around 10%. These results deomnstrate the high sensitivity of the CJP model to crack tip position and justify the necessity of using the methodology proposed in the present paper. It also implies that the CJP model is successfully capturing local influences on the overall elastic field.

Fig. 11 shows the path followed by the optimisation algorithm, which has been superimposed on the specimen speckle image. It is particularly significant that the path followed by the algorithm-calculated crack tip position does not reach its final position via a straight line, as the algorithm path searches adjacent points to the crack tip until the coordinates are close to the optimum solution. Fig. 12a and 12b show the changes in the x and y crack tip coordinates during the iterative process, normalised as the ratio of the distance between their × and y distances and the optimum crack tip position divided by the crack length. These normalised values approach zero as the optimum crack tip position is reached. Fig. 12 essentially highlights the optimisation-path distances shown in Fig. 11.

5.2. Crack tip characterising parameters and crack tip location

The crack tip characterising parameters (stress intensity factors and T-stress) and the crack tip location were found for crack lengths between 3.4 mm and 9.4 mm (equivalent to values of normalised crack length of 0.17 and 0.47). As a check of the accuracy of the proposed technique, Fig. 13 plots values of the CJP driving force, K_F and the standard value of Mode I stress intensity factors, K_I, versus crack length. Both sets of data follow a very similar trend line, with an average relative difference between them of 2.63% (Table 3) and are also similar to the results reported by Nowell et al [37].

Although these stress intensity factors appear to be similar, it is important to highlight the significant advantages of the CJP approach, that include the fact that the effective driving force for crack growth, in the presence of plasticity-induced shielding, is directly given by the net driving force K_F - K_R; a geometry-independence of the calculation, at least for some standard specimen types; and a correlation of fatigue crack growth rate over a wider range than the Irwin-Paris value (see reference 23 for details).

An additional check is given in Fig. 14 by comparing the crack path determined by the optimisation technique introduced in the present paper, with the crack path determined by the crack tip displacement intersection method. They are superimposed on the speckle image of the specimen surface for the crack length values given in Table 3. The two crack paths show a very good level of agreement, with an average difference of 50 μm in terms of the Euclidean distance between crack tip positions determined by both techniques (0.98% difference when normalised by the crack length). Fig. 15 shows the relative difference between crack tip positions found by the two techniques as a function of crack length. It can be seen that the difference decreases with increase in crack length. Higher values at short crack lengths are reasonable since the crack tip singularity is less intense than in the case of longer cracks and it is also possible that the manufacturing process of the specimen notch generates residual stresses that may modify the singularity field. As noted earlier, however, the reason for performing this work is because the parameters in the CJP model are rather sensitive to variations of a few pixels in the crack tip position, particularly in the case of the x-coordinate, and 50 μm represents around 4 pixels for the camera system used in this work.

Computed non-singular T-stresses along the × and y directions are plotted in Fig. 16. Both parameters show similar trends and correspond with the expected results, since a negative sign in the crack growth direction corresponds with a lateral contraction of the specimen under axial traction loading, and the positive sign in the case of the crack opening direction also corresponds with traction loading.

Table 4 gives values of the CJP stress intensity parameters, the

optimised crack tip location, the value of the error function at the end of the optimisation process and the time taken by each algorithm. Values of the retardation K_R and shear K_S stress intensity factors agree with those obtained in previous work of the same alloy [31,37,38]. Computation times in all cases are around 1 min, with the GA taking around 92% of the total computation time, which is reasonable compared with values reported in other work [19,20].

6. Conclusions

A novel technique has been outlined in the present work that provides an accurate conjoint determination of the CJP stress intensity factors and the crack tip location. The most important innovation is that the process includes estimation of the precise crack tip location as an additional unknown in the mathematical optimisation. The technique uses a hybrid process that combines an initial optimisation using a genetic algorithm, followed by use of an interior point algorithm. Its utility has been demonstrated through analysis of crack tip displacement fields experimentally measured using 2D-DIC. The value of the proposed technique arises from the known sensitivity of the CJP model to crack tip position where small errors in crack tip location (several pixels) can lead to substantial errors in the crack tip characterising parameters obtained with the model. Although the methodology has been developed specifically for the CJP model and DIC data, the proposed hybrid method can be applied with any model of crack tip fields, any isotropic material and any experimental technique used to measure displacement. An extension of that technique to the analysis of 3D-DIC would require only minor modifications and it would be attractive in analysing out-of-plane crack tip phenomena (i.e. tearing mode singularity parameters). A major advantage of the approach lies in the possibility of easy automation as the crack tip characterisation process sometimes involves large user effort and time. Apart from crack tip field characterisation, the proposed method would be useful in any application that requires a precise crack tip location.

In the light of the demonstrated ability of the CJP model to account for the shielding effects of the plastic enclave that surrounds a growing fatigue crack, future work will explore how the shielding effects during fatigue crack growth can be better evaluated using the proposed methodology. In the view of authors this, combined with a better understanding of the interaction between, and origin of, the five CJP parameters (A - E), will contribute to an increased understanding of the factors contributing to plasticity-induced shielding and the mechanisms involved in variable amplitude load interaction.

Declaration of Competing Interest

The authors declare that they have no known competing financial interests or personal relationships that could have appeared to influence the work reported in this paper.

Acknowledgements

This work has been performed with financial support from the Junta de Andalucía through the research project “1380786” funded by the program “Proyectos de I + D + i en el Marco del Programa Operativo FEDER Andalucía 2014-2020. Convocatoria 2020”.

References

[1] Schreier H, Orteu J-J, Sutton MA, editors. Image Correlation for Shape, Motion and Deformation Measurements. Boston, MA: Springer US; 2009.
[2] Thomson W (Lord K. On the Thermoelastic, Thermomagnetic and Pyro-electric Properties of Matters. Philos Mag 1878;5:4–27.
[3] Brewster D. On the communication of the structure of doubly refracting crystals to glass, muriate of soda, flour spar and other substances by mechanical compression and dilatation. Philos Mag 1816;106:156–78.
[4] Sanford RJ, Dally JW. A general method for determining mixed-mode stress intensity factors from isochromatic fringe patterns. Eng Fract Mech 1979;621:621–33.
[5] Westergaard HM. Bearing pressures and cracks. J Appl Mech 1939;61:49–53.
[6] Irwin GR. Analysis of stresses and strains near the end of a crack traversing plate. J Appl Mech 1957;24:361–70.
[7] Williams ML. On the stress distribution at the base of a stationary crack. J Appl Mech 1957;24:109–14.
[8] Nurse AD, Patterson EA. Determination of predominantly mode-II stress intensity factors from isochromatic data. Fatigue Fract Eng Mater Struct 1993;16(12):1339–54. https://doi.org/10.1111/j.1460-2695.1993.tb00743.x.
[9] Muskhelishvili NI. Some Basic Problems of the Mathematical Theory of Elasticity. Springer Netherlands; 1977. https://doi.org/10.1007/978-94-017-3034-1.
[10] Pommier S, Hamam R. Incremental model for fatigue crack growth based on a displacement partitioning hypothesis of mode I elastic-plastic displacement fields. Fatigue Fract Eng Mater Struct 2007;30:582–98. https://doi.org/10.1111/j.1460-2695.2007.01128.x.
[11] Christopher CJ, James MN, Patterson EA, Tee KF. Towards a new model of crack tip stress fields. Int J Fract 2007;148(4):361–71. https://doi.org/10.1007/s10704-008-9209-3.
[12] Christopher CJ, James MN, Patterson EA, Tee KF. A quantitative evaluation of fatigue crack shielding forces using photoelasticity. Eng Fract Mech 2008;75(14):4190–9. https://doi.org/10.1016/j.engfracmech.2008.03.013.
[13] James MN, Christopher CJ, Lu YW, Patterson EA. Local crack plasticity and its influences on the global elastic stress field. Int J Fatigue 2013;46:4–15. https://doi.org/10.1016/j.ijfatigue.2012.04.015.
[14] Lopez-Crespo P, Shterenlikht A, Patterson EA, Yates JR, Withers PJ. The stress intensity of mixed mode cracks determined by digital image correlation. J Strain Anal Eng Des 2008;43(8):769–80.
[15] Yates JR, Zanganeh M, Tai YH. Quantifying crack tip displacement fields with DIC. Eng Fract Mech 2010;77(11):2063–76. https://doi.org/10.1016/j.engfracmech.2010.03.025.
[16] Vasco-Olmo JM, Diaz FA, Garcia-Collado A, Dorado-Vicente R. Experimental evaluation of crack shielding during fatigue crack growth using digital image correlation. Fatigue Fract Eng Mater Struct 2015;38:223–37. https://doi.org/10.1111/ffe.12136.
[17] Vasco-Olmo JM. Evaluación experimental del fenómeno de crack shielding inducido por plasticidad empleando técnicas ópticas de campo completo para la medida de tensiones y deformaciones. Universidad de Jaén 2014.
[18] Yoneyama S, Morimoto Y, Takashi M. Automatic evaluation of mixed-mode stress intensity factors utilizing digital image correlation. Strain 2006;42:21–9. https://doi.org/10.1111/j.1475-1305.2006.00246.x.
[19] Zanganeh M, Lopez-Crespo P, Tai YH, Yates JR. Locating the Crack Tip Using Displacement Field Data: A Comparative Study. Strain 2013;49:102–15. https://doi.org/10.1111/str.12017.
[20] Yang B, Wei Z, Díaz FA, Liao Z, James MN. New algorithm for optimised fitting of DIC data to crack tip plastic zone using the CJP model. Theor Appl Fract Mech 2021;113:102950. https://doi.org/10.1016/j.tafmec.2021.102950.
[21] Moré JJ. The Levenberg-Marquardt algorithm: Implementation and theory 1978:105–16. https://doi.org/10.1007/BFB0067700.
[22] Goldberg DE. Genetic algorithms in search, optimization, and machine learning. 1st ed. Boston, MA: Addison-Wesley Longman Publishing Co., Inc.,; 1989. https://doi.org/10.5555/534133.
[23] Wright SJ. Primal-Dual Interior-Point Methods. Soc Ind Appl Mathematics 1997. https://doi.org/10.1137/1.9781611971453.
[24] Coleman TF, Li Y. An interior trust region approach for nonlinear minimization subject to bounds. Siam J Optim 1996;6(2):418–45. https://doi.org/10.1137/0806023.
[25] Byrd RH, Gilbert JC, Nocedal J. A trust region method based on interior point techniques for nonlinear programming. Math Program Ser B 2000;89(1):149–85. https://doi.org/10.1007/PL00011391.
[26] Byrd RH, Hribar ME, Nocedal J. An interior point algorithm for large-scale nonlinear programming. SIAM J Optim 1999;9(4):877–900. https://doi.org/10.1137/S1052623497325107.

[27] Waltz RA, Morales JL, Nocedal J, Orban D. An interior algorithm for nonlinear optimization that combines line search and trust region steps. Math Program 2006; 107(3):391–408. https://doi.org/10.1007/s10107-004-0560-5.
[28] Nocedal J, Wright SJ. Numerical Optimization 2006. https://doi.org/10.1007/978-0-387-40065-5.
[29] Dantzig GB. Recent Advances in Linear Programming. Manage Sci 1956;2(2): 131–44. https://doi.org/10.1287/mnsc.2.2.131.
[30] Kuhn HW, Tucker AW. Nonlinear programming. Proc 2nd Berkeley Symp 1951: 481–92.
[31] Vasco-Olmo JM, James MN, Christopher CJ, Patterson EA, Diaz FA. Assessment of crack tip plastic zone size and shape and its influence on crack tip shielding. Fatigue Fract Eng Mater Struct 2016;39:969–81. https://doi.org/10.1111/ffe.12436.
[32] Vasco-Olmo JM, Diaz FA, Patterson EA. Experimental evaluation of shielding effect on growing fatigue cracks under overloads using ESPI. Int J Fatigue 2016;83: 117–26. https://doi.org/10.1016/j.ijfatigue.2015.10.003.
[33] Fletcher R, Powell MJD. A Rapidly Convergent Descent Method for Minimization. Comput J 1963;6(2):163–8. https://doi.org/10.1093/comjnl/6.2.163.
[34] Broyden CG. Quasi-Newton Methods and their Application to Function Minimisation. Math Comput 1967;21(99):368. https://doi.org/10.2307/2003239.
[35] Goldfarb D. A Family of Variable-Metric Methods Derived by Variational Means. Math Comput 1970;24(109):23. https://doi.org/10.2307/2004873.
[36] ASTM. E 647 - 00: Standard Test Method for Measurement of Fatigue Crack Growth Rates. Annu B ASTM Stand 1103 2000.
[37] Nowell D, Nowell SC. A comparison of recent models for fatigue crack tip deformation. Theor Appl Fract Mech 2019;103:6. https://doi.org/10.1016/j.tafmec.2019.102299.
[38] Yang B, Vasco-Olmo JM, Díaz FA, James MN. A more effective rationalisation of fatigue crack growth rate data for various specimen geometries and stress ratios using the CJP model. Int J Fatigue 2018;114:189–97. https://doi.org/10.1016/j.ijfatigue.2018.05.027.